17th World Conference on Earthquake Engineering, 17WCEE
Sendai, Japan - September 27th to October 2nd 2021

REAL-TIME HYBRID SIMULATION WITH NONLINEAR NUMERICAL SUBSTRUCTURES BASED ON STATE-SPACE MODELING

M. Hovmand[(1)], L. V. Andersen[(2)], G. Abbiati[(3)]

[(1)] *Structural Engineer, AFRY, Denmark, martin.hovmand@afry.com*
[(2)] *Professor, Department of Engineering, Aarhus University, Denmark, lva@cae.au.dk*
[(3)] *Assistant Professor, Department of Engineering, Aarhus University, Denmark, abbiati@cae.au.dk*

Abstract

Real- and fast-time hybrid simulation is used for structural testing of components with rate-dependent restoring force. In order to ensure a stable closed-loop simulation, the numerical substructure response must be computed within about 1-2 msec using a real-time computer. As a consequence, the majority of nonlinear finite-element environments conceived for soft-time computing cannot be reused. This argument motivated the development of a state-space simulation framework for hybrid testing compatible with real-time computing. Modularity is achieved by assembling nonlinear state-space finite-elements using a dual-assembly approach. The major advantage is that any element is associated with a simple ordinary differential equation. As a result, the automatic generation of real-time code is strongly simplified. The accuracy and stability of the framework are studied with numerical simulations. An experimental application demonstrates the effectiveness of the tool.

Keywords: Real-time hybrid simulation; state-space modeling; partitioned time integration; localized Lagrange multipliers; hysteretic nonlinearity.

1 Introduction

Hybrid simulation (HS) is used to investigate the response of structural prototypes subjected to realistic loading histories using hybrid models. The hybrid model combines a physical substructure (PS) and a numerical substructure (NS) that interact with each other in a real-time closed-loop simulation. Specifically, the PS is tested in the laboratory using servo-controlled actuators equipped with force transducers, while the NS is instantiated in a numerical simulation environment. HS entails less effort for performing seismic testing compared to shake tables [1].

If the PS restoring force is rate-dependent, it requires performing HS in fast- or real-time. This means performing HS with a testing time scale $1 \leq \lambda \leq 20$ indicatively. In order to ensure a stable closed-loop simulation, the NS response must be computed within about 1-2 msec using a real-time computer. As a consequence, the majority of nonlinear finite-element environments conceived for soft-time computing cannot be reused. This argument motivated the development of state-space HS algorithms, for which hard real-time implementations are straightforward. The work of Bursi and co-workers was pioneering in this sense since it proposed state-space models and Rosenbrock schemes to perform HS. Monolithic and partitioned algorithms are reported in [2] and [3], respectively. An extended study covering both types of schemes is reported in [4]. More recently, [5] proposed a state-space partitioned time integrator based on the Generalized-α scheme of [6]. Specifically, the algorithm couples state-space equations of PS and NS using a dual-assembly procedure based on classical Lagrange multipliers (CLM). Interface compatibility of state vector rates ensures a stable coupled simulation. The algorithm was implemented on a MATLAB xPC target and used to perform HS of a reinforced concrete bridge at EUCENTRE, Pavia, Italy. A major advantage of the framework is that interface forces represented by Lagrange multipliers can be used to feed an input-output dynamic identification algorithm that estimates the parameters of the PS online, as demonstrated in [7]. In addition, compared to the Rosenbrock schemes of [4], algorithmic damping can be tuned with a single parameter.

All partitioned time integrators reviewed so far assemble the equation of motion of the hybrid model by coupling PS and NS state-space models. Such an approach requires manually harnessing nonlinear evolutionary equations of hysteretic forces and reduced-order substructure matrices. The procedure is time-consuming, and verification is not robust. Also, none of the described schemes allow for imposing time-

varying Dirichlet boundary conditions, which are necessary, for example, to implement multi-support excitation. In response to these two limitations, this paper describes a newly conceived HS algorithm that utilizes a partitioned approach to assembling the state-space equation of motion of the hybrid model. State-space elements, instead of substructures, are coupled using the localized Lagrange multiplier (LLM) approach [8]. Compared to the CLM, the LLM leads to a unique set of compatibility equations to describe the coupling between elements. As a result, the Steklov-Poincaré operator utilized to solve the equation of motion with a two-stage solution approach is unique and non-singular. The advantage is that the user simply specifies element connectivity matrices in a finite-element fashion. In addition, time-varying Dirichlet boundary conditions can be set to implement multi-support excitation in seismic HSs.

The paper is organized as follows. Section 2 describes the state-space partitioned algorithm, while Section 3 discusses numerical validation and Section 4 experimental validation. Section 5 summarizes conclusions and future outlooks.

2 The state-space partitioned scheme

In the proposed framework, the equation of motion of the hybrid model is obtained via dual-assembly of element equations given in the state-space form. Likewise, for a single generic element, the equation of motion reads,

$$M\dot{X}+R(X)=F(t)+B\Lambda \tag{1}$$

with,

$$X=\begin{bmatrix} u \\ v \\ s \end{bmatrix}, M=\begin{bmatrix} I & 0 & 0 \\ 0 & m & 0 \\ 0 & 0 & I \end{bmatrix}, R=\begin{bmatrix} -v \\ r(u,v,s) \\ g(u,v,s) \end{bmatrix}, F(t)=\begin{bmatrix} 0 \\ f(t) \\ 0 \end{bmatrix} \tag{2}$$

u, v and s specify vectors for displacement, velocity, and additional state variables; u and v always come as a pair in second-order mechanical systems, while s gathers all state-variables that model nonlinearities with memory such as, e.g. hysteresis; m is the mass matrix of the element, whereas I and 0 are identity and zero matrices, respectively; $r(u,v,s)$ describes the nonlinear restoring force vector, whereas $g(u,v,s)$ gathers the evolutionary equations pertaining to s. Finally, $f(t)$ is the externally applied load. The Lagrange multipliers Λ enforce compatibility with the other elements, as described in the Boolean connectivity matrix B. The method of localized Lagrange multipliers is used to assemble a set of element state-space elements of index $i \in \{1,..,n\}$ as defined in (1) to form the equation of motion of the hybrid model. The equation of motion of the hybrid model coincides to the following differential-algebraic equation (DAE),

$$M^{(i)}\dot{X}^{(i)}+R^{(i)}(X^{(i)})=F^{(i)}(t)+B^{(i)}\Lambda^{(i)} \tag{3a}$$

$$G^{(i)}\dot{X}^{(i)}+\overline{G}^{(i)}\dot{X}^{g}=0 \tag{3b}$$

$$\overline{G}^{c}\dot{X}^{g}=h(t) \tag{3c}$$

$$\sum_{i=1}^{n}\left(\overline{B}^{(i)}\Lambda^{(i)}\right)+\overline{B}^{c}\Lambda^{c}=0 \tag{3d}$$

where (3a) is an instance of (1) for element i-th; (3b) expresses the compatibility between each element i-th and the set of generalized interface degrees-of-freedom (DoFs); (3c) enforces state trajectories $h(t)$ on a subset of the hybrid model DoFs. Accordingly, $\dot{X}^{g}$ gathers all state-space element DoFs subjected to Dirichlet boundary conditions expressed by (3b) and (3c). Coupled DoFs (3b) are taken once without repetition. Finally (3d) enforces interface force balance among state-space finite-elements. Connectivity matrices are defined as,

$$G^{(i)}=\left[l^{(i)^T} \quad 0\right], \overline{G}^{(i)}=\left[\bar{l}^{(i)}\right], \overline{G}^c=\left[\bar{l}^c\right] \tag{4a}$$

$$B^{(i)}=\left[0 \quad l^{(i)^T}\right]^T, \overline{B}^{(i)}=\left[\bar{l}^{(i)^T}\right], \overline{B}^c=\left[\bar{l}^{c^T}\right] \tag{4b}$$

where $l^{(i)}$ and $\bar{l}^{(i)}$ collocate interface DoFs on state-space finite-elements. For a comprehensive description of how matrices $l^{(i)}$ and $\bar{l}^{(i)}$ are formulated, the reader is referred to the original work of [8]. The additional matrix $\bar{l}^c$ identifies the subset of $\dot{X}^g$ subjected to imposed trajectories $h(t)$.

The proposed state-space partitioned algorithm utilizes the trapezoidal rule scheme to integrate the response of a generic element. The procedure for integrating (3) with a time-step $\Delta t=t_{k+1}-t_k$ utilizes a two-stage solution approach. The basic idea, is that the coupled response of the hybrid model, which satisfies interface force balance (Neuman BCs) and compatibility (Dirichlet BCs) is obtained as the superposition of *free* and *link* solutions,

$$X_{k+1}^{(i)}=X_{k+1,f}^{(i)}+X_{k+1,l}^{(i)} \tag{5a}$$

$$\dot{X}_{k+1}^{(i)}=\dot{X}_{k+1,f}^{(i)}+\dot{X}_{k+1,l}^{(i)} \tag{5b}$$

The trapezoidal rule scheme is used to compute the *free* solution, which neglects Dirichlet BCs,

$$\widetilde{X}_{k+1,f}^{(i)}=X_k^{(i)}+\dot{X}_k^{(i)}\Delta t(1-\gamma) \tag{6a}$$

$$\dot{X}_{k+1,f}^{(i)}=D^{(i)^{-1}}\left(F_{k+1}^{(i)}-R^{(i)}\left(\widetilde{X}_{k+1,f}^{(i)}\right)\right) \tag{6b}$$

$$X_{k+1,f}^{(i)}=\widetilde{X}_{k+1,f}^{(i)}+\dot{X}_{k+1,f}^{(i)}\Delta t\gamma \tag{6c}$$

The *link* solution is obtained via linearization of (3),

$$X_{k+1,l}^{(i)}=D^{(i)^{-1}}B^{(i)}\Lambda_{k+1}^{(i)}\Delta t\gamma \tag{7a}$$

$$\dot{X}_{k+1,l}^{(i)}=D^{(i)^{-1}}B^{(i)}\Lambda_{k+1}^{(i)} \tag{7b}$$

where the dynamic tangent stiffness $D^{(i)}$ reads,

$$D^{(i)}=M^{(i)}+K_0^{(i)}\Delta t\gamma \tag{8}$$

For numerical elements, $R^{(i)}\left(\widetilde{X}_{k+1,f}^{(i)}\right)$ is an analytical expression, and $K_0^{(i)}=\dfrac{\partial R^{(i)}\left(X_0^{(i)}\right)}{\partial X^{(i)}}$ is computed using complex-step differentiation [9]. For physical elements, $R^{(i)}\left(\widetilde{X}_{k+1,f}^{(i)}\right)$ contains the measured restoring force $r^{(i)}$, and $K_0^{(i)}$ is assembled based on the initial tangent stiffness $k^{(i)}=\dfrac{\partial r^{(i)}\left(u_0^{(i)}\right)}{\partial u^{(i)}}$ and damping $c^{(i)}=\dfrac{\partial r^{(i)}\left(\dot{u}_0^{(i)}\right)}{\partial \dot{u}^{(i)}}$ matrices. If (6-7) is substituted into (5), the expression of Lagrange multipliers and generalized interface state reads,

$$\begin{bmatrix} \Lambda_{k+1}^{(1)} \\ \vdots \\ \Lambda_{k+1}^{(n)} \\ \Lambda_{k+1}^{c} \\ \dot{x}_{k+1}^{g} \end{bmatrix}=\begin{bmatrix} G^{(1)}D^{(1)^{-1}}B^{(1)} & \cdots & 0 & 0 & \overline{G}^{(1)} \\ \vdots & \ddots & \vdots & \vdots & \vdots \\ 0 & \cdots & G^{(n)}D^{(n)^{-1}}B^{(n)} & \vdots & \overline{G}^{(n)} \\ 0 & \cdots & \cdots & 0 & \overline{G}^{c} \\ \overline{B}^{(1)} & \cdots & \overline{B}^{(n)} & \overline{B}^{c} & 0 \end{bmatrix}^{-1}\begin{bmatrix} -G^{(1)}\dot{X}_{k+1,f}^{(1)} \\ \vdots \\ -G^{(n)}\dot{X}_{k+1,f}^{(n)} \\ h\left(t_{k+1}\right) \\ 0 \end{bmatrix}=H^{-1}\begin{bmatrix} -G^{(1)}\dot{X}_{k+1,f}^{(1)} \\ \vdots \\ -G^{(n)}\dot{X}_{k+1,f}^{(n)} \\ h\left(t_{k+1}\right) \\ 0 \end{bmatrix} \tag{9}$$

where H is the so-called Steklov-Poincaré operator, which maps Dirichlet to Neuman BCs by means of a linearization of the DAE in (3).

Based on this premise, the procedure for integrating (3) from t_k to t_{k+1} is summarized as a sequence of steps:

1) For each element i-th, solve the *free* problem at t_{k+1} using (6)
2) Solve the interface problem at t_{k+1} using (9)
3) For each element i-th, solve the *link* problem at t_{k+1} using (7)
4) Compute the coupled solution using (5).

The order of accuracy of the proposed partitioned state-space time integrator is computed numerically considering a linear split-mass system. The corresponding initial value problem reads,

$$\begin{bmatrix} 1 & 0 & 0 & 0 \\ 0 & 1 & 0 & 0 \\ 0 & 0 & m_1^{(1)} & 0 \\ 0 & 0 & 0 & m_2^{(1)} \end{bmatrix} \begin{bmatrix} \dot{u}_1^{(1)} \\ \dot{u}_2^{(1)} \\ \dot{v}_1^{(1)} \\ \dot{v}_2^{(1)} \end{bmatrix} + \begin{bmatrix} 0 & 0 & -1 & 0 \\ 0 & 0 & 0 & -1 \\ k^{(1)} & -k^{(1)} & 0 & 0 \\ -k^{(1)} & k^{(1)} & 0 & 0 \end{bmatrix} \begin{bmatrix} u_1^{(1)} \\ u_2^{(1)} \\ v_1^{(1)} \\ v_2^{(1)} \end{bmatrix} = \begin{bmatrix} 0 \\ 0 \\ f_1^{(1)}(t) \\ f_2^{(1)}(t) \end{bmatrix} + B^{(1)} \Lambda^{(1)} \tag{10a}$$

$$\begin{bmatrix} 1 & 0 & 0 & 0 \\ 0 & 1 & 0 & 0 \\ 0 & 0 & m_1^{(2)} & 0 \\ 0 & 0 & 0 & m_2^{(2)} \end{bmatrix} \begin{bmatrix} \dot{u}_1^{(2)} \\ \dot{u}_2^{(2)} \\ \dot{v}_1^{(2)} \\ \dot{v}_2^{(2)} \end{bmatrix} + \begin{bmatrix} 0 & 0 & -1 & 0 \\ 0 & 0 & 0 & -1 \\ k^{(2)} & -k^{(2)} & 0 & 0 \\ -k^{(2)} & k^{(2)} & 0 & 0 \end{bmatrix} \begin{bmatrix} u_1^{(2)} \\ u_2^{(2)} \\ v_1^{(2)} \\ v_2^{(2)} \end{bmatrix} = \begin{bmatrix} 0 \\ 0 \\ f_1^{(2)}(t) \\ f_2^{(2)}(t) \end{bmatrix} + B^{(2)} \Lambda^{(2)}$$

$$G^{(1)} = \begin{bmatrix} 1 & 0 & 0 & 0 \\ 0 & 1 & 0 & 0 \end{bmatrix}, \overline{G}^{(1)} = -\begin{bmatrix} 1 & 0 & 0 \\ 0 & 1 & 0 \end{bmatrix}, B^{(1)} = \begin{bmatrix} 0 & 0 \\ 0 & 0 \\ 1 & 0 \\ 0 & 1 \end{bmatrix}, \overline{B}^{(1)} = -\begin{bmatrix} 1 & 0 \\ 0 & 1 \\ 0 & 0 \end{bmatrix} \tag{10b}$$

$$G^{(2)} = \begin{bmatrix} 1 & 0 & 0 & 0 \\ 0 & 1 & 0 & 0 \end{bmatrix}, \overline{G}^{(2)} = -\begin{bmatrix} 0 & 1 & 0 \\ 0 & 0 & 1 \end{bmatrix}, B^{(2)} = \begin{bmatrix} 0 & 0 \\ 0 & 0 \\ 1 & 0 \\ 0 & 1 \end{bmatrix}, \overline{B}^{(2)} = -\begin{bmatrix} 0 & 0 \\ 1 & 0 \\ 0 & 1 \end{bmatrix}$$

$$\overline{G}^{c} = -\begin{bmatrix} 1 & 0 & 0 \\ 0 & 0 & 1 \end{bmatrix}, \overline{B}^{c} = -\begin{bmatrix} 1 & 0 \\ 0 & 0 \\ 0 & 1 \end{bmatrix}$$

where parameter values read,

$$m_1^{(1)} = m_2^{(1)} = m_1^{(2)} = m_2^{(2)} = 0.5, k^{(1)} = k^{(2)} = 0.5$$

Convergence is evaluated w.r.t. to a reference to y_1 at $t_{ref} = 0.1$ sec computed using the monolithic trapezoidal rule time integration scheme with a time step $\Delta t_{ref} = 1 \times 10^{-6}$ sec. The corresponding plot is reported in Figure 1. As can be observed from the plot, the scheme is 2nd order accurate.

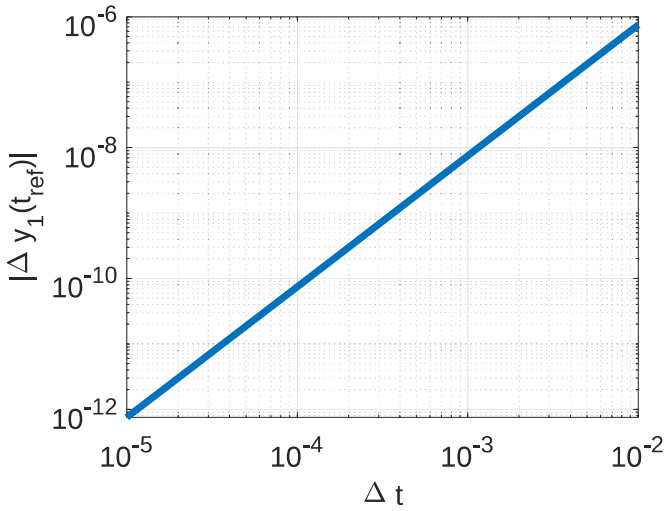

Fig. 1 - Convergence of the partitioned time integration scheme.

3 Numerical validation

3.1 Reference case study

The proposed scheme is benchmarked numerically and experimentally using the case study depicted in Figure 2. As can be appreciated from the figure, the benchmark case study consists of a cantilever beam (PS) connected to a nonlinear Bouc-Wen spring (NS). A sinusoidal displacement trajectory $h(t)$ is imposed to the free end of the spring. For a comprehensive review of Bouc-Wen-type springs see [10].

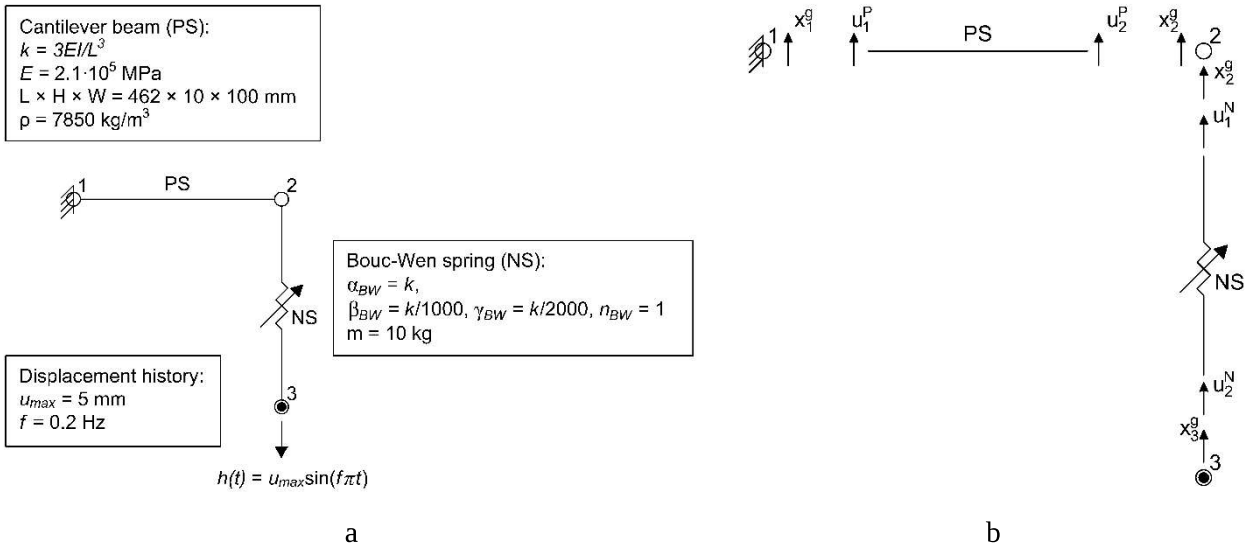

Fig. 2 – Benchmark case study: a) experimental properties; b) exploded view with internal displacement components.

Following the DAE (3) the state-space NS element of the hybrid model is defined as,

$$\begin{bmatrix} 1 & 0 & 0 & 0 & 0 & 0 \\ 0 & 1 & 0 & 0 & 0 & 0 \\ 0 & 0 & m_1^N & 0 & 0 & 0 \\ 0 & 0 & 0 & m_2^N & 0 & 0 \\ 0 & 0 & 0 & 0 & 1 & 0 \\ 0 & 0 & 0 & 0 & 0 & 1 \end{bmatrix} \begin{bmatrix} \dot{u}_1^N \\ \dot{u}_2^N \\ \dot{v}_1^N \\ \dot{v}_2^N \\ \dot{r}^N \\ \dot{e}^N \end{bmatrix} + \begin{bmatrix} -v_1^N \\ -v_2^N \\ r^N \\ -r^N \\ -\left(A - \left[\beta\, sign\left(r^N\left[v_1^N - v_2^N\right]\right) + \gamma\right]\left|r^N\right|^n\right)\left(v_1^N - v_2^N\right) \\ r\left(v_1^N - v_2^M\right) \end{bmatrix} = \begin{bmatrix} 0 \\ 0 \\ f_1^N(t) \\ f_2^N(t) \\ 0 \\ 0 \end{bmatrix} \tag{11}$$

where A is the elastic stiffness, while β, γ and n determine the shape of the hysteretic loop of the restoring force of the nonlinear spring. Similarly, the state-space PS element (the cantilever beam) is defined as,

$$\begin{bmatrix} 1 & 0 & 0 & 0 \\ 0 & 1 & 0 & 0 \\ 0 & 0 & m_1^P & 0 \\ 0 & 0 & 0 & m_2^P \end{bmatrix} \begin{bmatrix} \dot{u}_1^P \\ \dot{u}_2^P \\ \dot{v}_1^P \\ \dot{v}_2^P \end{bmatrix} + \begin{bmatrix} -v_1^P \\ -v_2^P \\ r^P \\ -r^P \end{bmatrix} = \begin{bmatrix} 0 \\ 0 \\ f_1^P(t) \\ f_2^P(t) \end{bmatrix} \tag{12}$$

Finally, for the sake of clarity, all connectivity matrices are provided for this example,

$$G^N = \begin{bmatrix} 1 & 0 & 0 & 0 & 0 & 0 \\ 0 & 1 & 0 & 0 & 0 & 0 \end{bmatrix}, \overline{G}^N = -\begin{bmatrix} 0 & 1 & 0 \\ 0 & 0 & 1 \end{bmatrix}, B^N = \begin{bmatrix} 0 & 0 \\ 0 & 0 \\ 1 & 0 \\ 0 & 1 \\ 0 & 0 \\ 0 & 0 \end{bmatrix}, \overline{B}^N = \begin{bmatrix} 0 & 0 \\ 1 & 0 \\ 0 & 1 \end{bmatrix} \tag{13a}$$

$$G^P = \begin{bmatrix} 1 & 0 & 0 & 0 \\ 0 & 1 & 0 & 0 \end{bmatrix}, \overline{G}^P = -\begin{bmatrix} 1 & 0 & 0 \\ 0 & 1 & 0 \end{bmatrix}, B^P = \begin{bmatrix} 0 & 0 \\ 0 & 0 \\ 1 & 0 \\ 0 & 1 \end{bmatrix}, \overline{B}^P = -\begin{bmatrix} 1 & 0 \\ 0 & 1 \\ 0 & 0 \end{bmatrix} \tag{13b}$$

$$\overline{G}^c = -\begin{bmatrix} 1 & 0 & 0 \\ 0 & 0 & 1 \end{bmatrix}, \overline{B}^c = -\begin{bmatrix} 1 & 0 \\ 0 & 0 \\ 0 & 1 \end{bmatrix} \tag{13c}$$

3.2 Error propagation analysis

The PS restoring force is contaminated with measurement noise, which propagates through the HS. Accordingly, an uncertainty propagation analysis of this noise is performed numerically considering RMS values calibrated on the experimental setup described in Section 4.1. In this regard, Figure 3 and 4 collects 100 realizations of the HS response simulated numerically to a reference deterministic simulation. As can be appreciated, noise has little effect on the displacement response of the hybrid model.

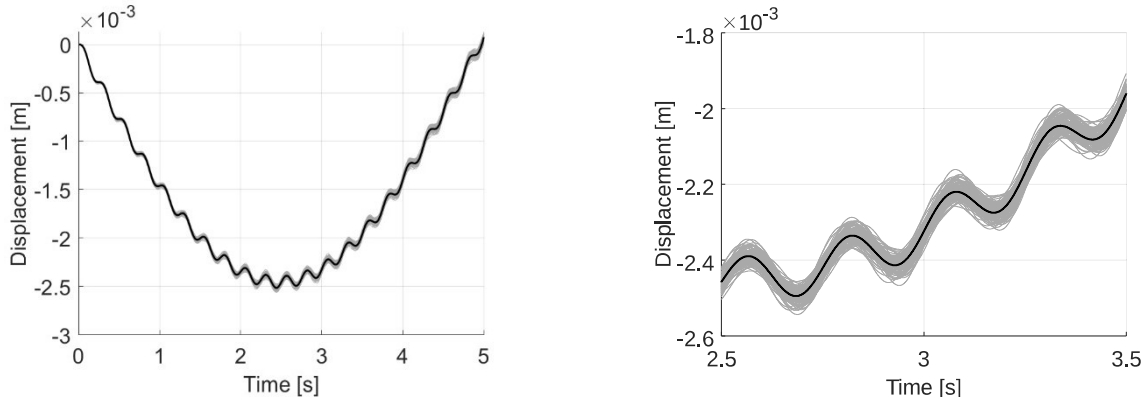

a b

Fig. 3 – Displacement response of the hybrid model with and w/o measurement noise: a) full time history; b) close up view on a mid-segment.

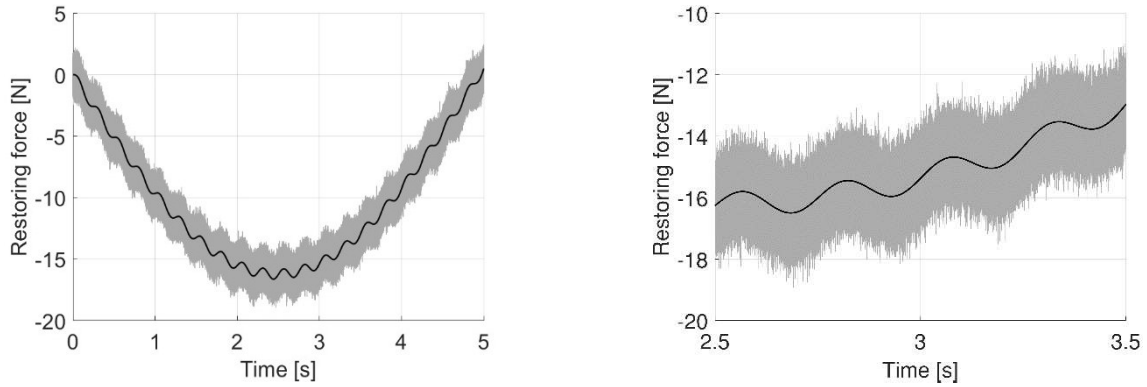

a b

Fig. 4 – Restoring force response of the hybrid model with and w/o measurement noise: a) full time history; b) close up view on a mid-segment.

4 Experimental validation

4.1 Hybrid simulation setup

The experimental validation of the proposed HS framework was performed using the same benchmark case study described in Section 3.1. A newly conceived HS setup installed at the Dynamisk LAB of Aarhus University was used for this purpose. In this regard, Figure 5 provides an overview of the experimental setup and the real-time system. The shown experimental setup, has a steel cantilever beam as a PS. The displacement of the simulated system is imposed on the PS by an electromechanical actuator, where a force transducer between the actuator and the PS measures the restoring force. The experimental setup runs on a Beckhoff RT-industrial PC, using TwinCAT to execute PLC code. This software uses the EtherCAT protocol for communication allowing for a processing-on-the-fly approach. The model execution parameters are then defined in Simulink from the details of the PLC task, as a discrete solver with fixed time steps, with a prolonged timeframe in the pseudo-dynamic time range, with $\lambda = 50$. The time step is defined as a multiple of the PLC execution rate corresponding to $10\,ms$.

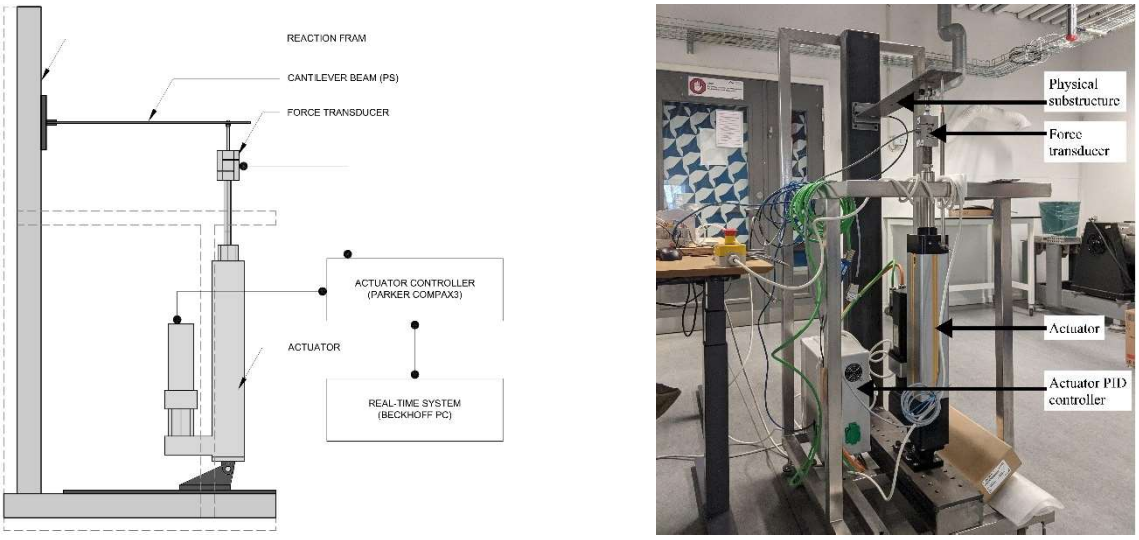

a b

Fig. 5 - HS setup at Dynamisk LAB, Aarhus University.

As part of the numerical framework, a MATLAB parser was implemented to automatically generate the SIMULINK model for real-time code generation compatible with the Beckhoff system. Figure 6 provides an overview of the automatically generated SIMULINK model for the hybrid model. Blue and red bounding boxes indicate portions of the SIMULINK model allocated for PS and NS state-space elements. The solution block computes both free and link solutions based on state-space element outputs. For a thorough description of the experimental implementation the reader is referred to [11].

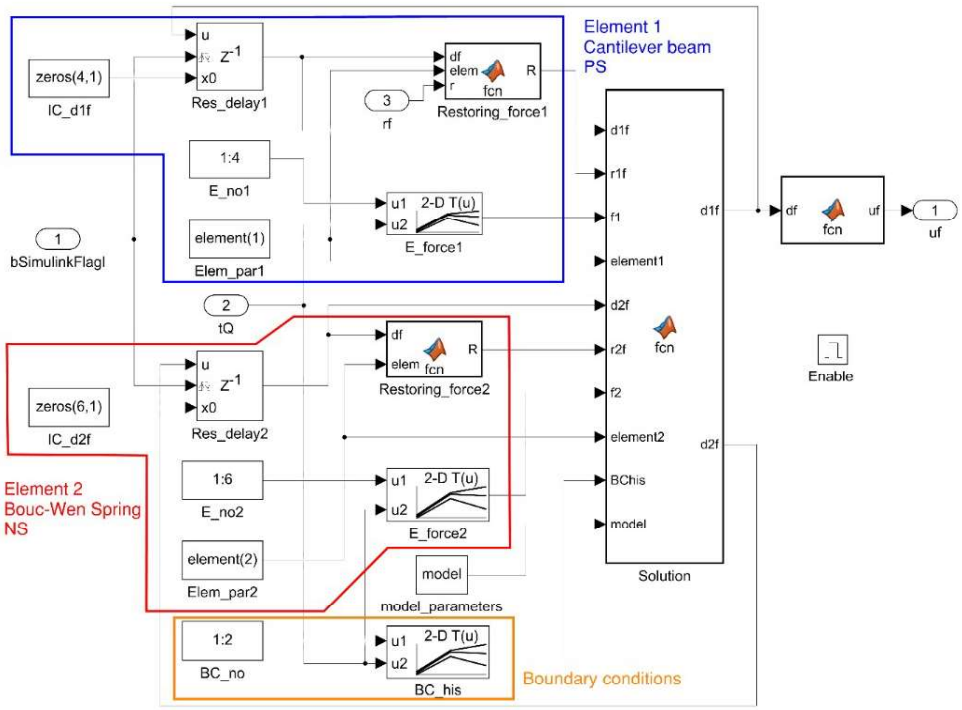

Fig. 6 – Automatically generated SIMULINK model for real-time code generation.

4.2 Results and discussion

Figure 7 summarizes the results of 4 HSs in terms of displacement and restoring force response histories. For clarity, experimental results are compared to a numerical reference simulation performed using the nominal stiffness of the PS computed with Bernoulli beam theory. Results indicate a slight overestimation of the PS stiffness in the reference numerical simulation. The repeatability of experiments is consistent with the error propagation analysis reported in Section 3.2. However, quantization noise is remarkably suggesting that the force measurement range should be reduced to increase the resolution of signals.

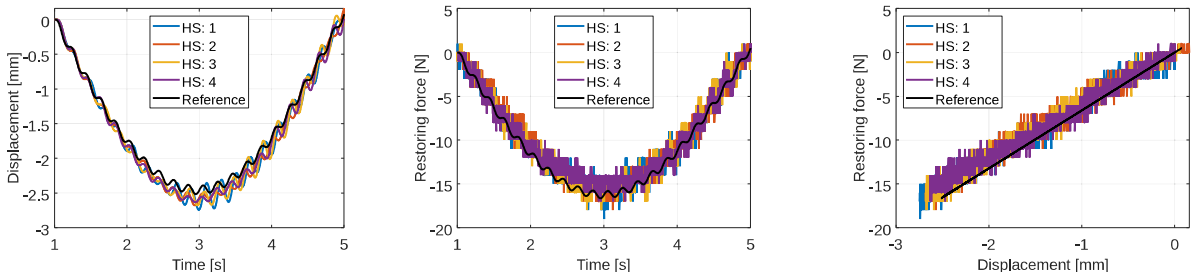

a b c

Fig. 7– HS simulation results a) Time displacement; b) Time restoring force diagram; c) Displacement restoring force diagram

Conclusions and future work

This paper presented a hybrid simulation algorithm based on partitioned time integration and state-space modelling. Specifically, the partitioned time integration scheme utilizes the localized Lagrange multiplier method to couple finite-elements defined by state-space equations to form substructures. The main advantage of partitioned time integration is that Dirichlet boundary conditions can be imposed without the need for Newton iterations. This is particularly useful to simulate multi-support excitation in seismic hybrid simulations. Compared to the classical Lagrange multiplier method, the localized Lagrange multiplier method provides a unique solution for the Steklov-Poincaré operator. This simplifies the implementation for the automatic assembly of coupling equations. Finally, state-space modelling enables using a wide range of phenomenological models for hysteretic restoring forces mainly developed in the field of dynamic identification, which are well-suited for hard real-time computations. The proposed algorithm utilizes the trapezoidal rule as a basic monolithic solver for the partitioned scheme. Notably, the algorithm is energy preserving for Hamiltonian systems.

The hybrid simulation algorithm was validated with an experimental case study, where the physical substructure was linear while the numerical substructure was nonlinear. The experiment was conducted using a newly conceived single-degree-of-freedom hybrid simulation setup installed at the Dynamisk LAB of Aarhus University.

Future work will be dedicated to introducing algorithmic dissipation using a generalized-α scheme as a basic solver. The advantage is that high frequency eigenmodes spuriously excited by experimental errors can be damped out.

Acknowledgements

The authors wish to acknowledge the assistance in realization of the experimental setup, provided by the technical staff of the Civil and Architectural Engineering Department of Aarhus University. Also, Beckhoff GmbH is greatly acknowledged for assisting the implementation of the real-time system.

References

[1] P. Pan, T. Wang and M. Nakashima, Development of online hybrid testing: Theory and Applications to Structural Engineering, Elsevier / Butterworth Heinemann, 2016.

[2] O. S. Bursi, A. Gonzalez-Buelga, L. Vulcan, S. A. Neild and D. J. Wagg, "Novel coupling Rosenbrock-based algorithms for real-time dynamic substructure testing," *Earthquake Engineering & Structural Dynamics*, vol. 37, no. 3, pp. 339-360, 2008.

[3] O. S. Bursi, C. Jia, L. Vulcan, S. A. Neild and D. J. Wagg, "Rosenbrock-based algorithms and subcycling strategies for real-time nonlinear substructure testing," *Earthquake Engineering & Structural Dynamics*, vol. 40, no. 1, pp. 1-19, 2011.

[4] O. S. Bursi, Z. Wang, C. Jia and B. Wu, "Monolithic and partitioned time integration methods for real-time heterogeneous simulations," *Computational Mechanics*, vol. 52, no. 1, 2013.

[5] G. Abbiati, I. Lanese, E. Cazzador, O. S. Bursi and A. Pavese, "A computational framework for fast-time hybrid simulation based on partitioned time integration and state-space modeling," *Structural Control and Health Monitoring*, pp. 1-28, 2019.

[6] K. E. Jansen, C. H. Whiting and G. M. Hulbert, "A generalized-α method for integrating the filtered Navier–Stokes equations with a stabilized finite element method," *Computer Methods in Applied Mechanics and Engineering*, 2000.

[7] G. Abbiati, I. Lanese, S. Eftekhar Azam, O. S. Bursi and A. Pavese, "A framework for hybrid simulation with online model updating suitable for hard real-time computing," *Structural Control and Health Monitoring*, p. e2652, 2020.

[8] K. C. Park, C. A. Felippa and U. A. Gumaste, "A localized version of the method of Lagrange multipliers and its applications," *Computational Mechanics*, vol. 24, no. 6, pp. 476-490, 2000.

[9] W. Squire and G. Trapp, "Using complex variables to estimate derivatives of real functions," *SIAM review*, vol. 40, no. 1, pp. 110-112, 1998.

[10] F. Ikhouane and J. Rodellar, "On the Hysteretic Bouc–Wen Model," *Nonlinear Dynamics*, vol. 42, pp. 79-95, 2005.

[11] M. Hovmand, "A state-space partitioned time integration scheme for hybrid simulation with multi-support excitation (Master's thesis)," *Aarhus University, Civil and Architectural Engineering*, 2021.

[12] J. C. Butcher, Numerical methods for ordinary differential equations, Wiley, 2008.

[13] A. Chopra, Dynamics of Structures: Theory and Applications to Earthquake Engineering, Saddle River, NJ: Prentice Hall. Inc., 1995.

[14] A. Gravouil and A. Combescure, "Multi-time-step explicit-implicit method for nonlinear structural dynamics," *International Journal of for Numerical Method in Engineering*, vol. 50, no. 1, p. 199–225, 2001.

[15] P. Pegon and G. Magonette, "Technical Report 1.02.167 "Continuous PSD testing with nonlinear substructuring: presentation of a stable parallel inter-field procedure"," European Commission, Joint Research Centre, ELSA, Ispra, Italy, 2002.

[16] A. Schellenberg, S. Mahin and G. Fenves, "Advanced Implementation of Hybrid Simulation," 2009.

